Optics Letters

Distribution of continuous variable quantum entanglement at a telecommunication wavelength over 20 km of optical fiber

Jinxia Feng,[1,2] Zhenju Wan,[1] Yuanji Li,[1,2] and Kuanshou Zhang[1,2,*]

[1]State Key Laboratory of Quantum Optics and Quantum Optics Devices, Institute of Opto-Electronics, Shanxi University, Taiyuan 030006, China
[2]Collaborative Innovation Center of Extreme Optics, Shanxi University, Taiyuan 030006, China
*Corresponding author: kuanshou@sxu.edu.cn

Received 13 June 2017; revised 27 July 2017; accepted 31 July 2017; posted 3 August 2017 (Doc. ID 298065); published 25 August 2017

The distribution of continuous variable (CV) Einstein–Podolsky–Rosen (EPR)-entangled beams at a telecommunication wavelength of 1550 nm over single-mode fibers is investigated. EPR-entangled beams with quantum entanglement of 8.3 dB are generated using a single nondegenerate optical parametric amplifier based on a type-II periodically poled $KTiOPO_4$ crystal. When one beam of the generated EPR-entangled beams is distributed over 20 km of single-mode fiber, 1.02 dB quantum entanglement can still be measured. The degradation of CV quantum entanglement in a noisy fiber channel is theoretically analyzed considering the effect of depolarized guided acoustic wave Brillouin scattering in optical fibers. The theoretical prediction is in good agreement with the experimental results.

OCIS codes: (270.0270) Quantum optics; (270.6570) Squeezed states; (270.5565) Quantum communications.

https://doi.org/10.1364/OL.42.003399

Continuous variable (CV) quantum entanglement is an essential resource for quantum computation and communication protocols [1]. The use of CV quantum entanglement at the telecommunication wavelength, in combination with existing fiber telecommunication networks, offers the possibility to implement long-distance quantum communication protocols such as quantum key distribution (QKD) [2] and applications such as quantum repeaters [3] and quantum teleportation [4] in the future. The quantum entanglement distribution is important if we are to realize large-scale quantum communication networks [5]. It is well known that the optical power attenuation of light in a standard telecommunication fiber is the lowest at the wavelength of 1550 nm. Numerous experiments have been reported on entanglement distribution, swapping, and teleportation in the 1550 nm wavelength band over optical fibers in a discrete variable regime [6–8]. Meanwhile, CV quantum communication over fiber channels has attracted much interest in recent years, due to the potential improvement of the channel capacity [9]. For example, the tolerance of the excess noise in the quantum channel can be enhanced significantly for CV QKD if CV quantum entanglement is used [10]. However, quantum entanglement is known to sensitively respond to environment influences, which unavoidably gives rise to quantum entanglement degradation [11]. Hence, the development of CV quantum state distribution through the quantum channel, especially in the optical fiber channel, is a demanding task. The propagation of CV entangled states in lossy channels and the distribution of squeezed states in free space have been experimental studied [12,13]. A few theoretical studies regarding the distribution of CV quantum entanglement over the optical fiber channel were reported [14,15], and a preliminary experimental test was performed on the distribution of entangled modes with 1 km of single-mode fiber in the Ph.D. dissertation by Händchen [16].

In this Letter, we investigate the distribution of the generated CV quantum entanglement at the telecommunication wavelength of 1550 nm over single-mode-fibers. The degradation of the quantum entanglement is theoretically analyzed considering the effect of the depolarized guided acoustic wave Brillouin scattering (GAWBS) in a single-mode fiber.

A scheme for the quantum entanglement distribution is that Alice holds EPR-entangled beams, and one beam of the EPR-entangled beams is distributed to Bob through a quantum channel [17,18]. The Duan's inseparability criterion of EPR-entangled beams is $\varepsilon_{ab} < 2$ [19]. After one beam is distributed over an optical fiber, ε_{ab} of EPR-entangled beams with anticorrelated amplitude quadratures and correlated phase quadratures can be given by

$$\begin{aligned}\varepsilon_{ab} &= \langle \delta(\hat{X}_a + \hat{X}'_b)^2 + \delta(\hat{Y}_a - \hat{Y}'_b)^2 \rangle \\ &= \langle \delta\hat{X}_a^2 \rangle + \langle \delta\hat{X}_b'^2 \rangle + 2\langle \delta\hat{X}_a \delta\hat{X}'_b \rangle \\ &\quad + \langle \delta\hat{Y}_a^2 \rangle + \langle \delta\hat{Y}_b'^2 \rangle - 2\langle \delta\hat{Y}_a \delta\hat{Y}'_b \rangle, \end{aligned} \tag{1}$$

where $\hat{X}_a$, $\hat{X}_b$ and $\hat{Y}_a$, $\hat{Y}_b$ are the amplitudes and phase quadratures of the EPR-entangled beams, modes a and b, respectively. X'_b and Y'_b are, respectively, the amplitude and phase quadrature of the distributed mode b over an optical fiber.

The optical mode transmitted over an ideal lossy fiber channel that there is only vacuum noise induced by loss can be written as

$$\hat{\alpha}_{\text{out}} = \sqrt{T}\hat{\alpha}_{\text{in}} + \sqrt{1-T}\hat{\nu}, \tag{2}$$

where $\hat{\alpha}_{\text{out}}$, $\hat{\alpha}_{\text{in}}$ are the output and input optical modes, respectively, and $\hat{\nu}$ is the vacuum noise. T is the transmission efficiency of the ideal lossy fiber channel. $T = T_1 10^{-\alpha L/10}$, T_1 is the fiber coupler efficiency, L is the length of the fiber, and α is the loss coefficient of the fiber, which is typically 0.2 dB/km at 1550 nm.

The excess noise in fiber channels has to be considered in the investigation of EPR-entanglement distribution. An important and troublesome excess noise in optical fibers is the thermal excitation of acoustic modes, called guided acoustic wave Brillouin scattering [20]. GAWBS, even though occurring at frequencies higher than 20 MHz, can constitute a significant thermal-noise source to the generation of squeezed states at low frequencies [21,22]. The mixed torsional–radial acoustic modes (TR_{2m}) of GAWBS change the polarization of light and cause a depolarized scattering of light [23]. In the scheme of CV quantum entanglement distribution, the local oscillator (LO) and one beam of EPR-entangled beams are polarization multiplexed into the fiber. The depolarized GAWBS can scatter a portion of LO photons into the EPR-entangled beam inevitably and constitute a thermal-noise source that will induce the degradation of quantum entanglement.

The optical mode transmitted over a noisy fiber channel in which the vacuum noise and excess noise are produced by the effect of the depolarized GAWBS in the fiber is given by [24]

$$\hat{\alpha}_{\text{out}} = \sqrt{\eta}\hat{\alpha}_{\text{in}} + \sqrt{(1-\eta)}\hat{\alpha}_G + \sqrt{1-\eta}\hat{\nu}, \tag{3}$$

where $\hat{\alpha}_G$ is the excess noise caused by the effect of the depolarized GAWBS. $\eta = (1 - \xi L)$, T is the transmission efficiency of the noisy fiber channel, and ξ is the photon scattering efficiency of the fiber due to the depolarized GAWBS.

The fluctuation of amplitude and phase quadratures of the distributed mode b over a noisy fiber channel can be given by

$$\begin{cases} \delta\hat{X}'_b = \sqrt{\eta}\delta\hat{X}_b + \sqrt{(1-\eta)}\delta\hat{X}_G + \sqrt{1-\eta}\delta\hat{X}_\nu \\ \delta\hat{Y}'_b = \sqrt{\eta}\delta\hat{Y}_b + \sqrt{(1-\eta)}\delta\hat{Y}_G + \sqrt{1-\eta}\delta\hat{Y} \end{cases}, \tag{4}$$

where δX_G, δX_ν, δY_G, and δY_ν are fluctuations of amplitude and phase quadratures of the depolarized GAWBS field and the vacuum in the noisy fiber channel, respectively.

In this case, ε_{ab} can be rewritten as

$$\begin{aligned} \varepsilon_{ab} &= \delta(\hat{X}_a + \hat{X}'_b)^2 + \delta(\hat{Y}_a - \hat{Y}'_b)^2 \\ &= \delta\hat{X}_a^2 + \delta\hat{Y}_a^2 + \eta(\delta\hat{X}_b^2 + \delta\hat{Y}_b^2) \\ &\quad + 2\sqrt{\eta}(\delta\hat{X}_a\delta\hat{X}_b - \delta\hat{Y}_a\delta\hat{Y}_b) \\ &\quad + (1-\eta)(\delta\hat{X}_G^2 + \delta\hat{X}_V^2 + \delta\hat{Y}_G^2 + \delta\hat{Y}_V^2). \end{aligned} \tag{5}$$

For the depolarized GAWBS field and, considering the fact that $\xi L \ll 1$, $\langle\delta\hat{X}_G^2\rangle = \langle\delta\hat{Y}_G^2\rangle \approx \xi L\bar{n}_{\text{LO}}$ in Ref. [24]. $\bar{n}_{\text{LO}}$ is the average photon number of the LO. For the vacuum, $\langle\delta\hat{X}_\nu^2\rangle = \langle\delta\hat{Y}_\nu^2\rangle = 1$. For the EPR-entangled beams with anticorrelated amplitude quadratures and correlated phase quadratures, the following relation is satisfied [25]:

$$\begin{aligned} \delta(\hat{X}_a + \hat{X}_b)^2 &= \delta(\hat{Y}_a - \hat{Y}_b)^2 = 2e^{-2r} \\ \delta\hat{X}_{a(b)}^2 &= \delta\hat{Y}_{a(b)}^2 = \cosh(2r) \\ \delta\hat{X}_a\delta\hat{X}_b &= -\sqrt{\cosh^2(2r) - 1} \\ \delta\hat{Y}_a\delta\hat{Y}_b &= \sqrt{\cosh^2(2r) - 1}, \end{aligned} \tag{6}$$

where r is the correlation parameter of EPR-entangled beams.

After one mode is distributed over a noisy fiber channel, the inseparability criteria of the EPR-entangled beams are theoretically calculated using Eq. (5) versus transmission length (L) of single-mode fibers with different photon scattering efficiencies (ξ) [Fig. 1, solid curve (a–d)] or with different LO powers [Fig. 1, dashed curve (i–iv)]. Curve (a) corresponds to $\xi = 0$ which means in an ideal lossy fiber channel. Curves (b–d) correspond to $\xi = 0.8 \times 10^{-12}$ cm^{-1}, 1.2×10^{-12} cm^{-1}, and 2.55×10^{-12} cm^{-1}, respectively, which are the typical values for the photon scattering efficiency of the acoustic modes (TR_{21}, TR_{23}, and TR_{25}) of GAWBS in a single-mode fiber with the core diameter of 125 μm and coating diameter of 245 μm [24]. r is set as 0.956, which corresponds to correlation variances of 8.3 dB of the EPR-entangled beams below the corresponding shot noise level (SNL). The LO power is 12 mW. Curves (i–iv) correspond to LO powers of 3, 6, 12, and 20 mW, and r and ξ are set as 0.956 and 1.2×10^{-12} cm^{-1}. It can be seen that ε_{ab} is increasing when L, ξ, or the LO power are increasing.

The experimental setup of the generation and distribution of CV quantum entanglement is shown in Fig. 2. The pump laser source is a fiber laser with an output power of 2.0 W and a continuous-wave single-frequency operation at 1550 nm. The laser beam was sent through a mode clear (MC) to filter the excess intensity noise of the laser. The main portion of the 1550 nm laser from the MC was frequency doubled to obtain a 775 nm laser that acted as the pump of the nondegenerate optical parametric amplifier (NOPA). The residual portion was used as the injected signal of the NOPA and LOs of homodyne detections. EPR-entangled beams with anticorrelated amplitude quadratures and correlated phase quadratures were generated from a triply resonant NOPA based on a type-II periodically poled $KTiOPO_4$ crystal when the relative phase between the pump and injected signal was locked to π. EPR-entangled beams with frequencies that are identical to that of the injected signal and polarized orthogonally to each other, were separated to beams a and b using a polarizing beam splitter (PBS1). Alice held the generated EPR-entangled beams and reserved one mode (beam a). Another mode (beam b) and LO were distributed to Bob over a single-mode fiber. The waist

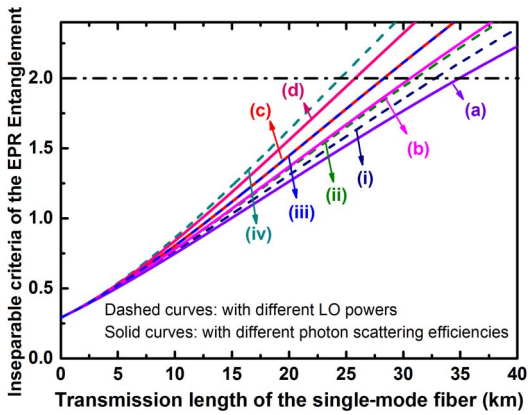

Fig. 1. Inseparability criteria of the EPR-entangled beams versus the transmission length of single-mode fibers with different photon scattering efficiencies [solid curve (a–d)] or with different LO powers [dashed curve (i–iv)].

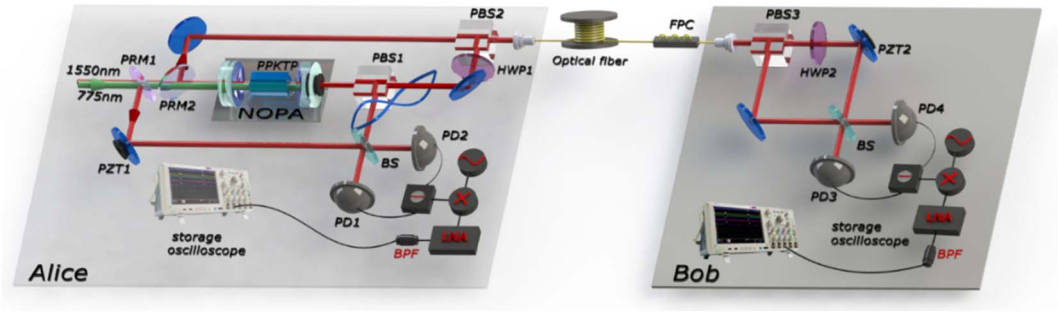

Fig. 2. Experimental setup of the generation and distribution of CV quantum entanglement. NOPA, nondegenerate optical parametric amplifier; PRM1-2, partial reflection mirror; PZT1-2, piezo-electric transducer; PBS1-3, polarizing beam splitter; BS, 50/50 beam splitter; PD1-4, photo detector; ⊖, negative power combiner; ⊗ , mixer; BPF, bandpass filter; LNA, low-noise amplifier; FPC, fiber polarization controller.

of the LO was transformed to be similar to that of beam b by a telescope system at first. Then, beam b and LO were combined on PBS2 and coupled into the single-mode fiber using an aspheric lens with a focus length of 11 mm. A fiber polarization controller was used to compensate for the polarization state variation induced by random fluctuations of birefringence of the single-mode fiber when the light propagates along the fiber, and to keep the polarization of light linear at the fiber output. After being distributed over a single-mode fiber, beam b and LO were separated by PBS3.

Alice and Bob simultaneously measure the amplitude and phase quadratures of beam a and distributed beam b, respectively, using homodyne detections. The sideband frequency of $\Omega = 7$ MHz was chosen as the center frequency for Alice's and Bob's measurements because the highest entanglement can be obtained at this frequency. The electric output signals from the negative power combiner (–) were passed through a low-noise amplifier with the gain of 30 dB and a bandpass filter (BPF) with the central frequency of 7 MHz and the bandwidth of 500 kHz, and recorded using a storage oscilloscope by Alice and Bob, respectively. However, there is a delay for beam b distributed over a single-mode fiber. The delay time is L/nc, c is the velocity of light, and n is the fiber's refractive index at 1550 nm. The recorded data were processed by a computer, including the synchronization and calculation of correlation variances of the distributed EPR-entangled beams.

The measured correlation variances of the amplitude sum and phase difference of the generated EPR-entangled beams from the NOPA are 8.44 ± 0.13 and 8.30 ± 0.11 dB below the corresponding SNL, respectively. The EPR-entangled beams satisfy the inseparability criterion $\langle \delta^2(\hat{X}_a + \hat{X}_b)\rangle + \langle \delta^2(\hat{Y}_a - \hat{Y}_b)\rangle = 0.29 \pm 0.02 < 2$. Beam b of the EPR-entangled beams and LO were distributed to Bob over single-mode fibers (SMF-28e) with lengths of 1, 2, 5, 10, 20, and 30 km. The amplitude (phase) quadratures were measured in a time domain when the relative phase between LO and EPR-entangled beam was locked to 0 ($\pi/2$). The SNLs were above the electronic noise levels of 4, 7, 10, and 12.2 dB at a frequency of 7 MHz when the LO powers were 3, 6, 12, and 20 mW, respectively. To get good signal-to-noise ratio at the homodyne detections, the optimized LO power was 12 mW in our experiment, although the theoretical calculation indicates that the distribution length of EPR-entangled beams is longer when the lower LO power is used.

Figure 3 shows the "global" perspectives of the Alice and Bob results measured on compatible bases when beam b of the EPR-entangled beams and LO was distributed over 10 km of single-mode fiber. Figures 3(a) and 3(b) show experimental data of the function of the amplitude quadratures (X_B versus X_A) and phase quadratures (Y_B versus Y_A). The sample rate of 2 MHz was chosen in the experiment, which corresponds to the measurement time of 5×10^{-7} s. The measurement time should be longer than the NOPA storage time of 4×10^{-8} s. (It equals the reciprocal of the NOPA optical cavity bandwidth of 25 MHz.) The quadrature measurements are normalized to the SNL of the measured beam. Figures 3(a) and 3(b) contain 50,000 data points. The anti-correlation of the amplitude quadratures and the correlation of the phase quadratures are clearly exhibited in the perspective. The measured correlation variances of the amplitude sum and phase difference of the distributed EPR-entangled beams are 3.56 ± 0.11 and 3.32 ± 0.11 dB below the corresponding SNL. The EPR-entangled beams satisfy the inseparability criterion of $0.91 \pm 0.02 < 2$.

Figure 4 shows the experimental data and theoretical prediction of inseparability criteria of the distributed EPR-entangled beams via the transmission length of the single-mode fiber. The diamonds in Fig. 4 are the experimental data. The first datum is the EPR inseparability criterion of the generated EPR-entangled beams. Other data are the inseparability criteria of EPR-entangled beams after beam b and LO are distributed to Bob over single-mode fibers with the fiber coupler efficiency of 88%. When beam b and LO are distributed to Bob over 20 km of single-mode fiber, the measured correlation variances

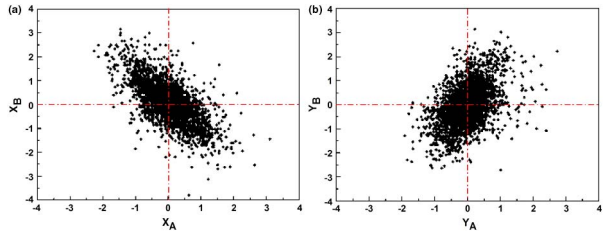

Fig. 3. "Global" perspectives of the Alice and Bob data. The curve (a) and (b) shows the function of the amplitude quadratures (X_B versus X_A) and phase quadratures (Y_B versus Y_A) for the distribution over 10 km of single-mode fiber.

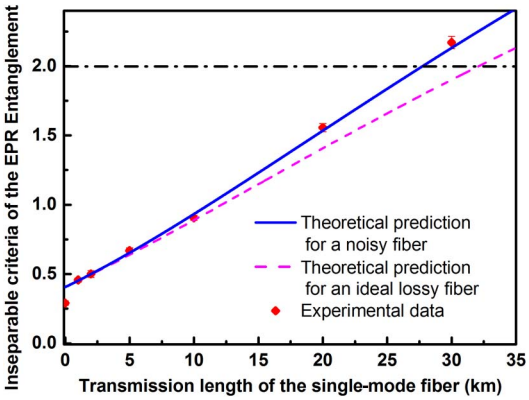

Fig. 4. Inseparability criteria of the EPR-entangled beams versus the transmission length of single-mode fibers. The diamonds are the experimental data. The solid and dashed curves are the theoretical prediction for a noisy fiber channel and an ideal lossy fiber channel.

of the amplitude sum and phase difference are, respectively, 1.16 ± 0.10 and 1.02 ± 0.11 dB below the corresponding SNL. The EPR inseparability criterion of 1.57 ± 0.03 is still less than 2. Furthermore, EPR-Reid criterion [26] was used to discuss the experimental results. The value of the EPR-Reid criterion is 0.91 which is less than 1, after beam b and LO are distributed to Bob over 20 km of single-mode fiber. Disentanglement is observed when beam b and LO are distributed to Bob over 30 km of single-mode fiber. The dashed line in Fig. 4 is the theoretical prediction considering the ideal lossy fiber channel. It can be seen that the discrepancy between the theoretical prediction and experimental results grows as the transmission length increases. The solid line in Fig. 4 is the theoretical prediction considering the noisy fiber channel, which is calculated using Eq. (5) with the parameters $\xi = 0.9 \times 10^{-12}\ \mathrm{cm}^{-1}$ and $T_1 = 88\%$, $\alpha = 0.2$ dB/km; quantum entanglement of the EPR-entangled beams is 8.3 dB, and the LO power is chosen to be 12 mW. The parameter ξ of $0.9 \times 10^{-12}\ \mathrm{cm}^{-1}$ is chosen to fit the experimental data because it is difficult to get the influence weight to the photon scattering efficiency from every acoustic mode of GAWBS in a single-mode fiber quantitatively. The theoretical prediction considering the excess noise in the fiber channel is in good agreement with the experimental results.

In conclusion, we have demonstrated the distribution of CV quantum entanglement at a telecommunication wavelength over 20 km of single-mode fiber. When LO and beam b of EPR-entangled beams with quantum entanglement of 8.3 dB are distributed to Bob over 20 km of single-mode fiber, the measured correlation variances of amplitude sum and phase difference are, respectively, 1.16 and 1.02 dB below the corresponding SNL. The EPR inseparability criterion of 1.57 is still less than 2. Using a theoretical model considering the excess noise induced by the depolarized GAWBS in a fiber channel, the theoretical prediction is in good agreement with the experimental results. The experimental results illustrate the potential for fiber-based CV quantum communication.

Funding. Key Project of the Ministry of Science and Technology of China (2016YFA0301401); National Natural Science Foundation of China (NSFC) (61227015, 11204167, 61405109).

REFERENCES

1. S. L. Braunstein and P. V. Loock, Rev. Mod. Phys. **77**, 513 (2005).
2. L. S. Madsen, V. C. Usenko, M. Lassen, and R. Filip, Nat. Commun. **3**, 1083 (2012).
3. H. J. Briegel, W. Dur, J. I. Cirac, and P. Zoller, Phys. Rev. Lett. **81**, 5932 (1998).
4. S. L. Braunstein and H. J. Kimble, Phys. Rev. Lett. **80**, 869 (1998).
5. H. J. Kimble, Nature **453**, 1023 (2008).
6. I. Marcikic, H. de Riedmatten, W. Tittel, H. Zbinden, M. Legre, and N. Gisin, Phys. Rev. Lett. **93**, 180502 (2004).
7. X. Li, P. L. Voss, J. Chen, J. E. Sharping, and P. Kumar, Opt. Lett. **30**, 1201 (2005).
8. R. Valivarthi, M. I. G. Puigibert, Q. Zhou, G. H. Aguilar, V. B. Verma, F. Marsili, M. D. Shaw, S. W. Nam, D. Oblak, and W. Tittel, Nat. Photonics **10**, 676 (2016).
9. A. S. Holevo and R. F. Werner, Phys. Rev. A **63**, 032312 (2001).
10. S. Pirandola, C. Ottaviani, G. Spedalieri, C. Weedbrook, S. L. Braunstein, S. Lloyd, T. Gehring, C. S. Jacobsen, and U. L. Andersen, Nat. Photonics **9**, 397 (2015).
11. L. M. Duan and G. C. Guo, Quantum Semiclassical Opt. **9**, 953 (1997).
12. F. A. S. Barbosa, A. S. Coelho, A. J. de Faria, K. N. Cassemiro, A. S. Villar, P. Nussenzveig, and M. Martinelli, Nat. Photonics **4**, 858 (2010).
13. C. Peuntinger, B. Heim, C. R. Müller, C. Gabriel, C. Marquardt, and G. Leuchs, Phys. Rev. Lett. **113**, 060502 (2014).
14. A. V. Chizhov, L. Knoll, and D. G. Welsch, Phys. Rev. A **65**, 022310 (2002).
15. F. A. S. Barbosa, A. J. de Faria, A. S. Coelho, K. N. Cassemiro, A. S. Villar, P. Nussenzveig, and M. Martinelli, Phys. Rev. A **84**, 052330 (2011).
16. V. Händchen, "Experimental analysis of Einstein–Podolsky–Rosen steering for quantum information applications," Ph.D. dissertation (Institute of Gravitational Physics, Leibniz University Hannover, 2016).
17. M. Curty, M. Lewenstein, and N. Lütkenhaus, Phys. Rev. Lett. **92**, 217903 (2004).
18. J. Lodewyck, M. Bloch, R. García-Patrón, S. Fossier, E. Karpov, E. Diamanti, T. Debuisschert, N. J. Cerf, R. Tualle-Brouri, S. W. McLaughlin, and P. Grangier, Phys. Rev. A **76**, 042305 (2007).
19. L. M. Duan, G. Giedke, J. I. Cirac, and P. Zoller, Phys. Rev. Lett. **84**, 2722 (2000).
20. R. M. Shelby, M. D. Levenson, and P. W. Bayer, Phys. Rev. B **31**, 5244 (1985).
21. M. Shirasaki and H. A. Haus, Opt. Lett. **17**, 1225 (1992).
22. J. F. Corney, P. D. Drummond, J. Heersink, V. Josse, G. Leuchs, and U. L. Andersen, Phys. Rev. Lett. **97**, 023606 (2006).
23. R. M. Shelby, M. D. Levenson, and P. W. Bayer, Phys. Rev. Lett. **54**, 939 (1985).
24. Y. M. Li, N. Wang, X. Y. Wang, and Z. L. Bai, J. Opt. Soc. Am. B **31**, 2379 (2014).
25. F. Grosshans and P. Grangier, Phys. Rev. Lett. **88**, 057902 (2002).
26. M. D. Reid and P. D. Drummond, Phys. Rev. Lett. **60**, 2731 (1988).